Applied Catalysis B: Environmental 170-171 (2015) 144–152

Contents lists available at ScienceDirect

Applied Catalysis B: Environmental

journal homepage: www.elsevier.com/locate/apcatb

$Ru_xTi_{1-x}O_2$ as the support for Pt nanoparticles: Electrocatalysis of methanol oxidation

M.D. Obradović[a], U.Č. Lačnjevac[b], B.M. Babić[c], P. Ercius[d], V.R. Radmilović[d,e], N.V. Krstajić[e], S.Lj. Gojković[e,*]

[a] Institute of Chemistry, Technology and Metallurgy, University of Belgrade, Njegoševa 12, 11000 Belgrade, Serbia
[b] Institute for Multidisciplinary Research, University of Belgrade, Kneza Višeslava 1, 11030 Belgrade, Serbia
[c] Vinča Institute of Nuclear Sciences, University of Belgrade, P.O. Box 522, 11001 Belgrade, Serbia
[d] National Center for Electron Microscopy, LBLN University of California, Berkeley, USA
[e] Faculty of Technology and Metallurgy, University of Belgrade, Karnegijeva 4, 11120 Belgrade, Serbia

ARTICLE INFO

Article history:
Received 14 September 2014
Received in revised form
29 December 2014
Accepted 30 January 2015
Available online 2 February 2015

Keywords:
Methanol oxidation
Platinum
TiO_2
RuO_2
Fuel cell

ABSTRACT

Two binary Ru–Ti oxides, $Ru_{0.1}Ti_{0.9}O_2$ and $Ru_{0.7}Ti_{0.3}O_2$, were synthesized by the sol–gel method and used as an electrocatalyst support. The system was characterized by XRD, EDS, TEM and cyclic voltammetry. The $Ru_{0.1}Ti_{0.9}O_2$ and $Ru_{0.7}Ti_{0.3}O_2$ consist of two phases of anatase and rutile structure. An average size of the Pt nanoparticles supported on them is ~3.5 nm and they are deposited on both Ru and Ti-rich domains. The supports exhibited good conductivity and electrochemical stability. The onset potentials of CO_{ads} oxidation on the synthesized catalysts and on commercial PtRu/C are similar to each other and lower than that on Pt/C. This suggests that in $Pt/Ru_{0.1}Ti_{0.9}O_2$ and $Pt/Ru_{0.7}Ti_{0.3}O_2$ the Pt nanoparticles are in close contact with Ru atoms from the support, which enables the bifunctional mechanism. The activity and stability of the catalysts for methanol oxidation were examined under potentiodynamic and potentiostatic conditions. While the activity of $Pt/Ru_{0.1}Ti_{0.9}O_2$ is unsatisfactory, the performance of $Pt/Ru_{0.7}Ti_{0.3}O_2$ is comparable to PtRu/C. For example, in the potentiostatic test at 0.5 V the activities after 25 min are 0.035 mA cm^{-2} and 0.022 mA cm^{-2} for $Pt/Ru_{0.7}Ti_{0.3}O_2$ and PtRu/C, respectively. In potentiodynamic test the activities at 0.5 V after 250 cycles are around 0.02 mA cm^{-2} for both catalysts.

1. Introduction

Current polymer electrolyte membrane fuel cell (PEMFC) technology employs carbon black as the anode and cathode catalyst support [1]. Although this kind of support possesses high electrical conductivity and high surface area necessary for fine dispersion of the catalyst particles, its oxidation under typical fuel cell operating conditions is inevitable [2–5]. Partial oxidation of carbon induces the formation of oxygen-containing functional groups on the surface that weakens Pt—C bond, thus facilitating surface diffusion of Pt nanoparticles and their agglomeration, especially in the case of the Pt nanoparticles smaller than 2 nm [6]. If the carbon support is oxidized to CO or CO_2, Pt nanoparticles detach from the surface [2]. Both processes reduce the electrochemically active surface area (EASA) of the catalyst system. The focus of recent research is to improve the catalyst stability by replacing carbon materials with metal oxides as the catalyst support [7,8]. Among the oxides, TiO_2 distinguishes itself due to high stability in acid media [9]. In the past several years TiO_2 has been successfully tested as a Pt catalyst support as a pure mesoporous oxide [10,11], doped by Nb [12–15] or as binary oxides such as $Ti_{0.7}W_{0.3}O_2$ [16], $Ru_xTi_{1-x}O_2$ [17], hydrous and anhydrous TiO_2–RuO_2 [18] and $Ti_{0.7}Ru_{0.3}O_2$ [19,20]. The addition of foreign atoms into the TiO_2 crystal lattice increases the conductivity of otherwise low-conducting TiO_2 but can also promote the catalyst activity, i.e., transform a catalyst support to a co-catalyst.

TiO_2 supports containing Ru are particularly interesting, because Pt-Ru surfaces are unsurpassed electrocatalysts for methanol oxidation reaction (MOR) owing to a combination of a bifunctional mechanism [21] and the electronic influence of Ru on Pt atoms [22]. According to bifunctional mechanism, Ru sites provide oxygen-containing species at less positive potentials than Pt, which facilitates oxidative removal of CO and other methanol residues from the Pt sites. Transfer of electron density from Pt to Ru, which can be comprehended as lowering of the d-band center of Pt [23], weakens the CO bonding to the Pt sites but also strengthens

* Corresponding author. Tel.: +381 11 3303 753; fax: +381 11 3370 387.
E-mail address: sgojkovic@tmf.bg.ac.rs (S.Lj. Gojković).

http://dx.doi.org/10.1016/j.apcatb.2015.01.038
0926-3373/

the bonding of OH and CO species to Ru sites [24]. The bifunctional mechanism is considered to be predominant over the electronic effect in the MOR promotion on Pt–Ru surfaces [25].

$Ru_xTi_{1-x}O_2$ (x between 0.17 and 0.75) prepared by the sol–gel routine [17] revealed that the samples with Ru mole fraction higher than 0.27 were electronically conductive after 30 min of heat treatment at 450 °C. Concerning the phase composition, a two phase mixture was found when the Ru mole fraction was below 0.5, while a solid solution was formed when the Ru fraction was higher than 0.5. The crystal structure corresponded to anatase for the oxides with $x < 0.25$ and to rutile at higher Ru fraction. Pt nanoparticles were supported on $Ru_xTi_{1-x}O_2$ (loading from 17 to 40 mass%) and examined by cyclic voltammetry. High Ru content was shown to increase the amount of electrochemically active surface area of Pt by a factor of two between the supports with $x = 0.27$ and $x = 0.71$.

X-ray diffraction (XRD) examination of hydrous RuO_2–TiO_2 prepared by a wet chemical method [18] showed only anatase TiO_2 without the features of RuO_2. After annealing at 450 °C two distinct phases of anatase TiO_2 and rutile RuO_2 were found, with no incorporation of Ru inside the TiO_2 crystallites. The annealing process i.e., phase structure of RuO_2–TiO_2 did not influence the particle size of the supported Pt. However, Pt catalysts on the annealed support presented better electrochemical stability. The Pt/RuO_2–TiO_2 samples in that study were also tested for oxygen reduction reaction (ORR). Although their activity was below the Pt/C benchmark, it is expected that optimization of the Pt particle size and electrode structure may make them suitable for the application in fuel cells.

Hydrothermal synthesis of $Ti_{0.7}Ru_{0.3}O_2$ performed at low temperature (200 °C) yielded a single phase solid solution with TiO_2 in the anatase form [19]. The material was hydrated with 0.23 mole of water per mole of $Ti_{0.7}Ru_{0.3}O_2$ and possessed BET surface area of 275 $m^2\,g^{-1}$. The electrocatalytic activity of Pt nanoparticles supported on $Ti_{0.7}Ru_{0.3}O_2$ was examined for CO and methanol oxidation. Both reactions were significantly enhanced compared to Pt/C and PtRu/C, which was ascribed to the bifunctional mechanism owing to high proton conductivity of hydrated $Ti_{0.7}Ru_{0.3}O_2$. The same $Ti_{0.7}Ru_{0.3}O_2$ was also used as a supporting material for Pt nanowires and tested for ORR and MOR [20].

As literature survey showed that studies of TiO_2–RuO_2 oxides as the catalyst supports are scarce and that very few of them examined MOR on Pt supported on such materials, we synthesized $Ru_xTi_{1-x}O_2$ employing a sol-gel method followed by thermal treatment with the aim to be used as an active support for Pt in MOR. Two samples of $Ru_xTi_{1-x}O_2$ powder with $x = 0.1$ and $x = 0.7$ were prepared and modified by Pt nanoparticles. The Pt/$Ru_xTi_{1-x}O_2$ catalysts were tested for the activity towards CO and methanol oxidation.

2. Experimental procedures

2.1. Preparation of $Ru_xTi_{1-x}O_2$ and Pt/$Ru_xTi_{1-x}O_2$

The synthesis of the $Ru_xTi_{1-x}O_2$ powders was based on an acid-catalyzed sol–gel method proposed for TiO_2 nanoparticles [26] and modified by addition of Ru [27]. In 40 mL of 97% solution of titanium(IV) isopropoxide, $Ti[OCH(CH_3)_2]_4$ (Alfa Aesar) an appropriate amount of 0.82 mol dm^{-3} aqueous solution of $RuCl_3$ (Merck) is added to achieve the Ru:Ti atomic ratio of 0.1:0.9 and 0.7:0.3. Soles were prepared by adding a 0.9 cm^3 of 12 mol dm^{-3} HCl solution (Merck) to the mixture of Ti and Ru precursors under vigorous steering at room temperature. The mixtures were placed in glass tubes, sealed and left for 5 days at room temperature. In the presence of such amount of HCl, the hydrolysis proceeded without forming a precipitate, leading to a transparent sol. Gelification of the sol was achieved by adding an appropriate amount of water.

The samples were dried by a freeze-drying method using Modulyo Freeze Dryer System (Edwards) consisting of freeze dryer unit at High Vacuum Pump E 2 M 8 (Edwards). Samples were pre-frozen in the deep-freeze refrigerator at −30 °C for 24 h. After that, the samples were freeze-dried in an acrylic chamber with shelves mounted directly on the top of the condenser of the freeze dryer. The vacuum during freeze-drying was around 4 mbar. The dried samples were heated in a conventional furnace at 400 °C for 2 h to obtain crystallized phases and to remove traces of organic residues. After the treatment, the furnace was cooled at room temperature.

Pt/$Ru_xTi_{1-x}O_2$ catalysts with a nominal Pt loading of 20 mass% were prepared by modified borohydride reduction method [28]. 80 mg RuO_2–TiO_2 powders were dispersed in 80 mg of water in an ultrasonic bath. Then an appropriate volume of 10 mg cm^{-3} H_2PtCl_6 aqueous solution was added into suspension under continuous stirring. After adjusting the suspension pH to 10 by adding 0.1 mol dm^{-3} NaOH solution, the metal salt was slowly reduced in the presence of excess of 0.5 M $NaBH_4$ solution under continuous stirring at 40 °C. The precipitate was rinsed with water and dried at 80 °C in inert atmosphere.

2.2. Physico-chemical characterization

Adsorption and desorption isotherms of N_2 were measured on $Ru_xTi_{1-x}O_2$ supports at −196 °C using the gravimetric McBain method. The specific surface area, S_{BET}, was calculated from the isotherms using the Brunauer–Emmett–Teller (BET) method. Pore size distribution was estimated by applying the Barrett–Joyner–Halenda (BJH) method [29] to the desorption branch of the isotherms.

The phase composition of the $Ru_xTi_{1-x}O_2$ supports was investigated by XRD. A Siemens D-500 diffractometer was employed with CuKα radiation of wavelength 0.154056 nm in conjunction with a CuKβ nickel filter.

The average elemental composition of the $Ru_xTi_{1-x}O_2$ supports and the Pt/$Ru_xTi_{x-1}O_2$ catalysts was performed by energy-dispersive X-ray spectroscopy (EDS) using a scanning electron microscope Tescan VEGA TS 5130MM coupled with an EDS system INCAPentaFET-x3, Oxford Instruments.

Transmission electron microscopy (TEM) was employed to analyze the morphology and elemental distribution of the Pt/$Ru_xTi_{x-1}O_2$ catalysts. The samples were sonicated in ethanol and a drop of the suspension was placed on a Cu grid (300 mesh) covered by lacey carbon film and dried in air. A combination of high angle annular dark field scanning transmission electron microscopy (HAADF-STEM) and electron energy loss spectroscopy (EELS) was applied. HAADF-STEM image intensity has a strong correlation with atomic number making it easy to distinguish between heavy elements such as Pt and a light support such as $Ru_xTi_{x-1}O_2$. The measurements were performed on TEAM 0.5 TEM with aberration-correction operated at 80 kV accelerating voltage. EDS mapping was performed on a CM200-FEG TEM operating at 200 kV by using an Oxford Instruments EDS system with INCA software. Crystallographic information from individual Pt particles was obtained by numerical Fourier filtering (Fast Fourier Transformation, FFT) of the digital image intensity spectra. All TEM characterization was done at the National Center for Electron Microscopy, Lawrence Berkeley National Laboratory.

2.3. Electrochemical characterization

For the electrochemical characterization, the Pt/$Ru_xTi_{1-x}O_2$ catalysts were applied on a glassy carbon (GC) substrate in the form of a thin-film [30]. The GC electrode (Tacussel rotating disk electrode, 5 mm in diameter) was polished with Al_2O_3 slurry and washed ultrasonically with water before use. The ink was made by

mixing of 6.5 mg of $Pt/Ru_xTi_{x-1}O_2$ powder with 1 cm^3 of high purity water (Millipore, 18 MΩ cm resistivity) and 50 μL of the Nafion® solution (5 wt%, 1100 E.W., Aldrich). After 1 h of agitation in an ultrasonic bath, 10 μL of the suspension was placed onto the GC electrode and left to dry overnight. The Pt loading on the electrode was 65 μg cm^{-2} for both $Pt/Ru_xTi_{1-x}O_2$ catalysts.

Electrochemical characteristics of the $Pt/Ru_xTi_{1-x}O_2$ thin films were investigated by cyclic voltammetry in 0.1 M H_2SO_4 saturated by N_2. After immersion into the electrolyte, the electrode was subjected to 15 potential cycles between 0.04 and 1.0 V at the scan rate of 100 mV s^{-1}. The oxidation of CO_{ads} was examined in the same electrolyte after adsorbing CO at 0.1 V for 30 min and replacing CO by N_2 atmosphere.

The MOR was investigated in the electrolyte containing 0.5 M CH_3OH, which was added in the sulfuric acid solution while the potential was held at 0.1 V. After 2 min a linear sweep of 50 mV s^{-1} (potentiodynamic polarization curve) or potential step at 0.5 V vs. RHE (chronoamperometric experiment) was applied.

We used to following electrocatalysts as references: a sample of Pt nanoparticles supported on XC-72R carbon with a loading of 20 mass% of Pt (Pt/C) and a sample of PtRu nanoparticles supported on the same carbon with a loading of 20 mass% of PtRu (PtRu/C), both manufactured by E-Tek. The reported average diameters of Pt and PtRu particles were 2.5 nm [31] and 2.7 nm [32], respectively. The metal loading on the electrode was 20 μg cm^{-2} for both Pt/C and PtRu/C.

The EASA of Pt or PtRu was determined from the charge of the CO_{ads} oxidation, which was carried out prior to each MOR experiment. In that way MOR currents were normalized to EASA for that particular catalyst layer. EASA was also determined from the charge of the oxidation of underpotentially (upd) deposited Cu [33,34]. Cu was deposited from the supporting electrolyte containing 2 mM $CuSO_4$ at the potential of 0.33 V.

A three-compartment electrochemical glass cell was used with a Pt wire as the counter electrode and a saturated calomel electrode as the reference electrode. All the potentials reported in the paper are expressed on the scale of the reversible hydrogen electrode (RHE). A Pine RDE4 potentiostat and Philips PM 8143 X-Y recorder were used. All the measurements were carried out at 25 °C.

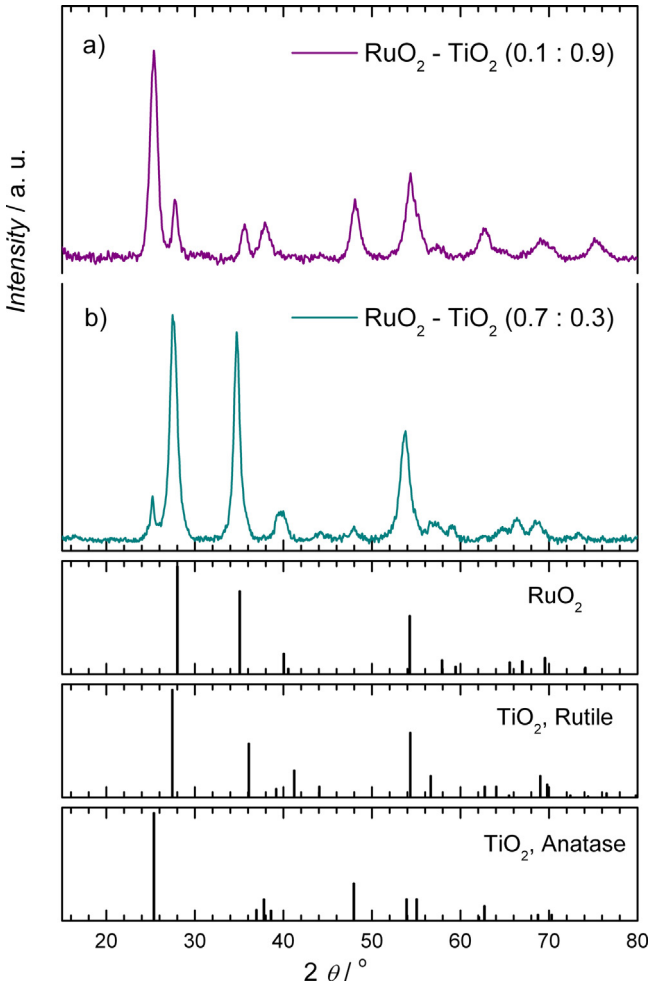

Fig. 1. XRD pattern of prepared supports RuO_2–TiO_2: (a) $Ru_{0.1}Ti_{0.9}O_2$; (b) $Ru_{0.7}Ti_{0.3}O_2$. The 2θ positions for bulk RuO_2, TiO_2, anatase and rutile structures, are shown on the plot for the reference.

3. Results and discussion

3.1. Physico-chemical characterization of $Ru_xTi_{1-x}O_2$ and $Pt/Ru_xTi_{1-x}O_2$

Analysis of N_2 adsorption and desorption isotherms (Fig. S1) showed that the BET surface areas of $Ru_xTi_{1-x}O_2$ supports with nominal composition of $x = 0.1$ and $x = 0.7$ were 41 and 33 m^2 g^{-1}, respectively. According to BJH pore size distribution, both samples are mesoporous with a pore radius mostly between 2 and 3 nm. Since the surface area of $Ru_xTi_{1-x}O_2$ powders is not very high, the small pore diameter indicates that the concentration of the pores within the material is rather low. BET surface areas of similar oxide supports reported in literature vary between 33 m^2 g^{-1} for anhydrous TiO_2–RuO_2 [18] and 276 m^2 g^{-1} for $Ti_{0.7}Ru_{0.3}O_2$ [19].

In order to find the average elemental composition of the $Pt/Ru_xTi_{x-1}O_2$ powders, EDS analysis was applied at five different places with surface area from about 20 × 20 μm to about 200 × 200 μm (Fig. S2). For the samples with low and high Ru content, the atomic ratios of Ru and Ti were found to be 0.08:0.92 and 0.68:0.32, respectively. Since these values are very close to the nominal Ru:Ti atomic ratio of 0.1:0.9 and 0.7:0.3, we denoted the samples as $Ru_{0.1}Ti_{0.9}O_2$ and $Ru_{0.7}Ti_{0.3}O_2$. The Pt content in the $Pt/Ru_{0.1}Ti_{0.9}O_2$ and $Pt/Ru_{0.7}Ti_{0.3}O_2$ catalysts was found to be 22.7 and 23.2 mass%, respectively, which corresponds to the nominal 20 mass% within the experimental error of EDS method.

XRD analysis was performed to determine the phase and crystal structure of the $Ru_xTi_{1-x}O_2$ supports. RuO_2 crystallize in a tetragonal rutile structure with the lattice constants $a = b = 0.44994$ nm, $c = 0.31071$ nm (JCPD card 43-10271). On the other side, TiO_2 crystallizes in two structures: anatase (lattice constants $a = b = 0.37854$ nm and $c = 0.94835$ nm; JCPD card 21-1272) and rutile structure (lattice constants $a = b = 0.45933$ nm and $c = 0.29592$ nm; JCPD card 21-1276). XRD patterns of the as-prepared oxides $Ru_{0.1}Ti_{0.9}O_2$ and $Ru_{0.7}Ti_{0.3}O_2$ are presented in Fig. 1 along with the reference spectra of RuO_2 and TiO_2. In both samples anatase and rutile peaks are present, but their intensities are different. Anatase peaks are predominant for $Ru_{0.1}Ti_{0.9}O_2$ (Fig. 1(a)) while rutile peaks are predominant for $Ru_{0.7}Ti_{0.3}O_2$ (Fig. 1(b)). As the peak positions of RuO_2 and TiO_2 rutile phases are very close to each other, it is hard to determine the composition of the rutile phase. For example, it is possible that all TiO_2 in $Ru_{0.1}Ti_{0.9}O_2$ is in a form of anatase and that rutile peaks belong to RuO_2, but it is also possible that a part of TiO_2 forms a solid solution with RuO_2 resulting in rutile peaks. In $Ru_{0.7}Ti_{0.3}O_2$ the intensity of the anatase peaks is relatively low, so TiO_2 is likely to be distributed within anatase and solid solution of TiO_2 in RuO_2. According to the phase diagram of RuO_2–TiO_2 system in air [35], at temperatures below 1400 K the solubility of TiO_2 in RuO_2, as well as solubility of RuO_2 in TiO_2 is less than 10 at%, which means that in $Ru_{0.7}Ti_{0.3}O_2$ single

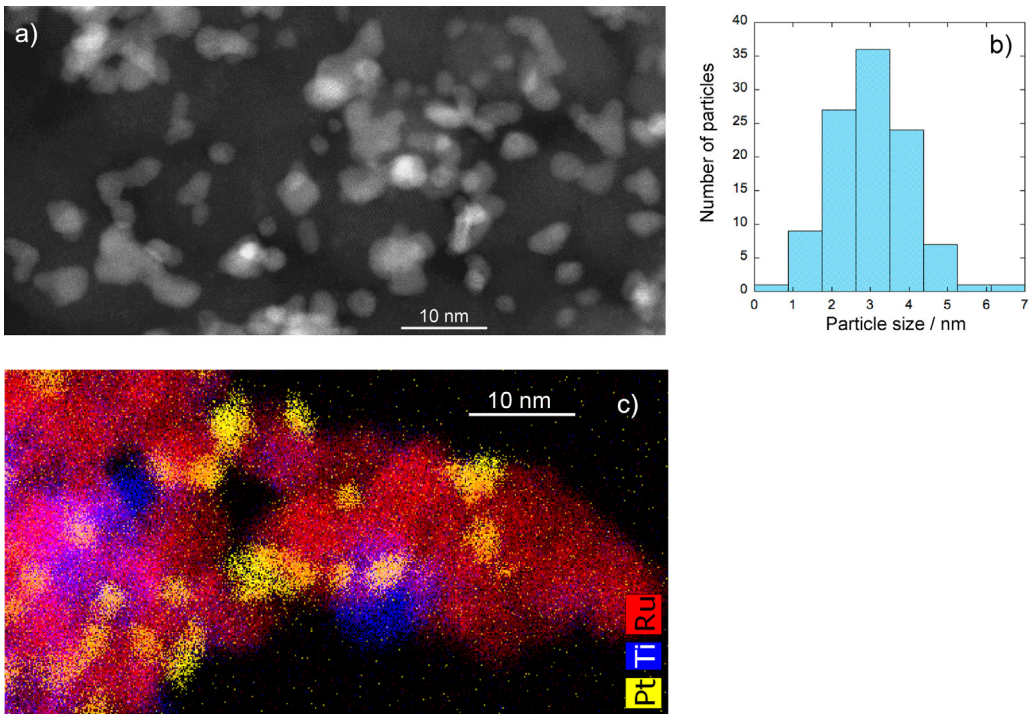

Fig. 2. (a) HAADF-STEM image of Pt particles/clusters on the $Ru_{0.7}Ti_{0.3}O_2$ support; (b) histogram of Pt particle size distribution and (c) EDS elemental mapping of $Pt/Ru_{0.7}Ti_{0.3}O_2$ catalyst.

phase solid solution of TiO_2 in RuO_2 is not thermodynamically stable. Thus, either two solid solutions of TiO_2 and RuO_2 are present, or $Ru_{0.7}Ti_{0.3}O_2$ contains metastable solid solution of TiO_2 in RuO_2. Here, it should be considered that phase diagrams relate to bulk phases, while the oxide samples examined are nano-sized particles.

HAADF-STEM image of $Pt/Ru_{0.7}Ti_{0.3}O_2$ presented in Fig. 2(a) shows that Pt particle and particle agglomerates are evenly distributed over the oxide support. Similar results with noticeable agglomeration of Pt particles were also obtained for $Pt/Ru_{0.1}Ti_{0.9}O_2$ (Figs. S3a and b). From the histograms of Pt particle size distribution (Fig. 2(a) and Fig. S3c) the surface-averaged diameter, $\bar{d}_s$, was calculated as

$$\bar{d}_s = \frac{\sum_{i=1}^{n} n_i d_i^3}{\sum_{i=1}^{n} n_i d_i^2} \quad (1)$$

where n_i stands for the number of particles having a diameter d_i. Only "isolated" (round shaped, not aggregated) Pt particles were taken into account. The surface-averaged diameter is the most relevant diameter in electrocatalysis [36] and was used for calculation of real surface area of Pt nanoparticles (RSA) according to equation:

$$\mathrm{RSA} = \frac{6}{\bar{d}_s \times \rho(\mathrm{Pt})} \quad (2)$$

where ρ(Pt) is density of Pt. The surface-averaged diameter for Pt nanoparticles in the $Pt/Ru_{0.1}Ti_{0.9}O_2$ and $Pt/Ru_{0.3}Ti_{0.7}O_2$ catalysts were found to be 3.4 nm and 3.7 nm, respectively, which correspond to RSA of 82 $m^2\ g^{-1}$ and 75 $m^2\ g^{-1}$ (Table 1).

EDS elemental mapping of the $Pt/Ru_{0.7}Ti_{0.3}O_2$ catalyst presented in Fig. 2(c) suggests that Pt is deposited on both Ru and Ti rich domains on the support with no preference for one over the other material. This implicates that most of the Pt particles are in contact with Ru due to the high Ru content in the support, which is a prerequisite for the bifunctional mechanism to be operative.

Table 1
Surface-averaged diameter ($\bar{d}_s$), real surface area (RSA), electrochemically active surface area (EASA) and utilization of the electroactive metal (η) for the synthesized and commercial catalysts.

	$Pt/Ru_{0.1}Ti_{0.9}O_2$	$Pt/Ru_{0.7}Ti_{0.3}O_2$	PtRu/C	Pt/C
$\bar{d}_s$/nm	3.4	3.7	2.7[a]	2.5[b]
RSA/$m^2\ g^{-1}$	82	75	92	112
EASA/$m^2\ g^{-1}$	17	32	131	76
η/%	21	43	70	68

[a] Ref. [32].
[b] Ref. [31].

3.2. Cyclic voltammetry of $Pt/Ru_xTi_{1-x}O_2$ and surface area determination

Steady-state cyclic voltammograms of the $Pt/Ru_{0.1}Ti_{0.9}O_2$ and $Pt/Ru_{0.7}Ti_{0.3}O_2$ catalysts are presented in Fig. 3 along with Pt/C and PtRu/C reference samples. It is clearly seen that the $Pt/Ru_{0.1}Ti_{0.9}O_2$ and $Pt/Ru_{0.7}Ti_{0.3}O_2$ profiles resemble Pt/C with well-defined peaks for hydrogen adsorption/desorption and a similar potential of Pt-oxide formation and reduction. Contrary to those three catalysts, the hydrogen adsorption/desorption region on PtRu/C voltammogram is featureless, which is a characteristic of the solid solution of Pt and Ru [32]. It can be concluded that no mixing between Pt and Ru occurred during preparation of $Pt/Ru_{0.1}Ti_{0.9}O_2$ and $Pt/Ru_{0.7}Ti_{0.3}O_2$ catalysts.

The cyclic voltammograms of the synthesized catalysts (Fig. 3(b) and (c)) are well centered and without inclination, demonstrating good conductivity of the $Ru_xTi_{1-x}O_2$ support. Besides, well-known pseudocapacitive behavior of Ru-oxide, which is present in the oxide supports, is manifested through higher current densities in

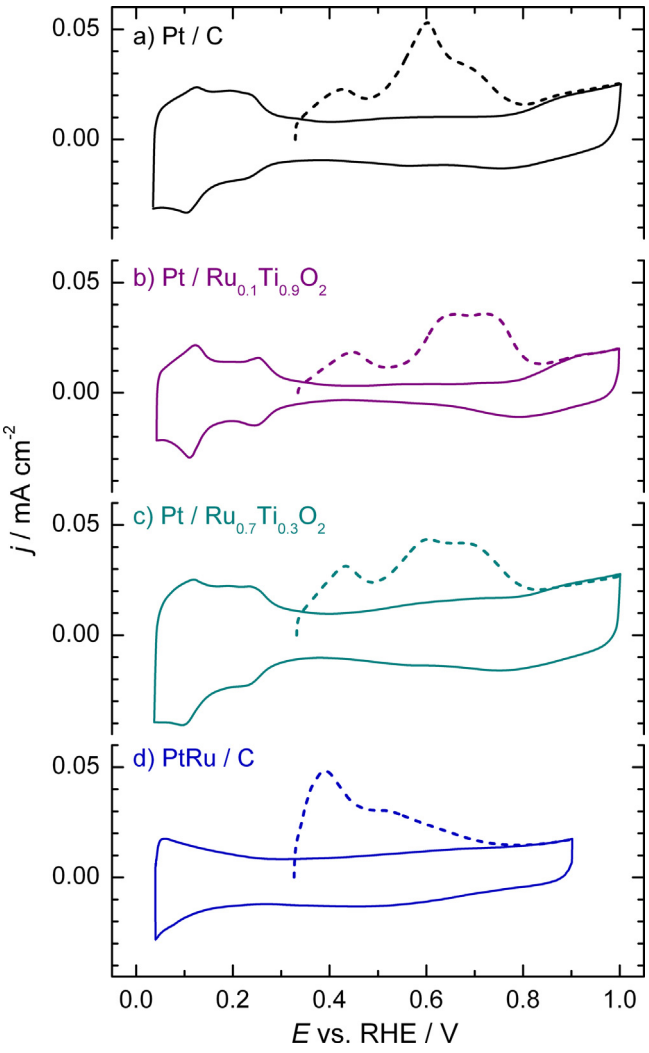

Fig. 3. Cyclic voltammograms of catalysts: (a) Pt/C, (b) $Pt/Ru_{0.1}Ti_{0.9}O_2$, (c) $Pt/Ru_{0.7}Ti_{0.3}O_2$ and (d) PtRu/C recorded in 0.10 M H_2SO_4 and upd Cu stripping voltammograms recorded in the presence of 2.0×10^{-3} M $CuSO_4$ (dashed lines). Scan rate 20 mV s^{-1}.

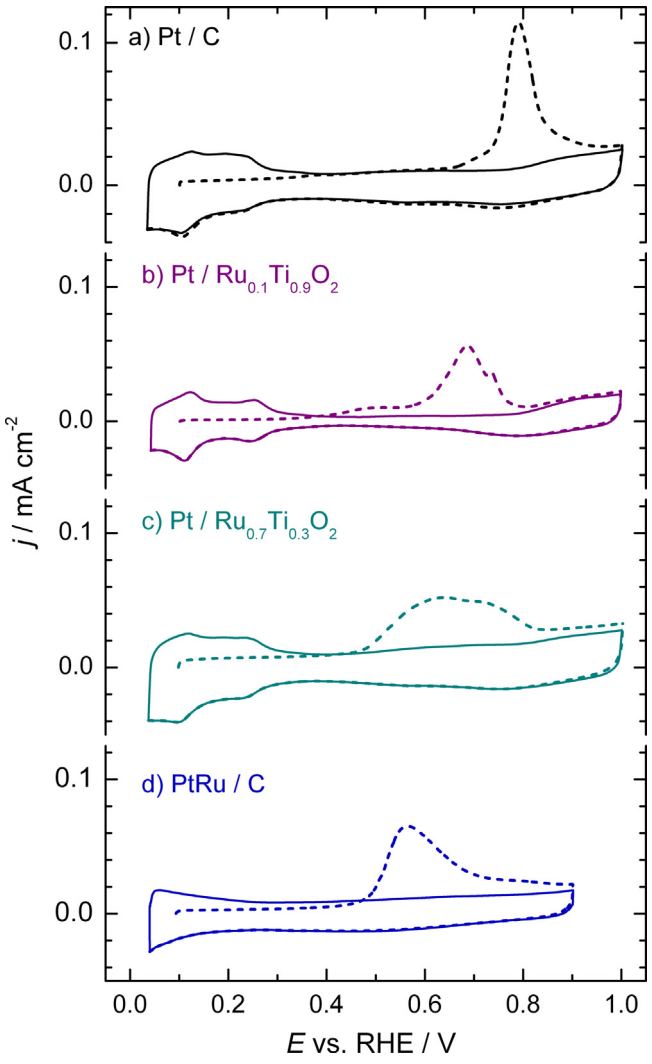

Fig. 4. Stripping voltammograms of CO_{ads} (dashed lines) and the first subsequent cyclic voltammograms (solid lines) of: (a) Pt/C, (b) $Pt/Ru_{0.1}Ti_{0.9}O_2$, (c) $Pt/Ru_{0.7}Ti_{0.3}O_2$ and (d) PtRu/C. Data recorded in 0.10 M H_2SO_4 at the scan rate of 20 mV s^{-1}.

so-called double layer region (between 0.3 V and 0.75 V) for Ru-rich $Pt/Ru_{0.7}Ti_{0.3}O_2$ comparing to $Pt/Ru_{0.1}Ti_{0.9}O_2$.

In order to compare surface characteristics of the catalysts and to determine their EASA, stripping voltammograms of upd layers of Cu are recorded and overlaid with the cyclic voltammograms of each catalyst (Fig. 3). Stripping voltammograms for Pt/C and PtRu/C are typical for this kind of catalysts [33,34]. Two peaks and a shoulder are observed for Pt/C indicating copper sites of different adsorption energies. On PtRu/C a Cu upd layer is striped through a peak at 0.4 V followed by a shoulder. The peak corresponds to Cu deposited on Ru atoms, while the shoulder originates in Cu deposited on Pt atoms [33]. The Cu stripping profiles for $Pt/Ru_{0.1}Ti_{0.9}O_2$ and $Pt/Ru_{0.7}Ti_{0.3}O_2$ are similar to each other and resemble Pt/C confirming that Pt and the supporting oxides exist in separate phases.

Since Cu deposits underpotentially on metallic Ru, but not on oxidized Ru sites [33], charge of upd Cu stripping corresponds to the EASA of Pt nanoparticles in Pt/C, $Pt/Ru_{0.1}Ti_{0.9}O_2$ and $Pt/Ru_{0.7}Ti_{0.3}O_2$ catalysts as well as to the EASA of PtRu nanoparticles in PtRu/C. For the calculation of the stripping charge a cyclic voltammogram in the supporting electrolyte was used as the base line. A ratio 1:1 of Cu atom to Pt and Ru site was assumed which gives a charge of 420 μC cm^{-2} for a monolayer of Cu [33].

Oxidation of pre-adsorbed CO on Pt follows Langmuir–Hinshelwood mechanism [37]:

$$CO_{ads} + OH_{ads} = CO_2 + H^+ + e^- \quad (3)$$

according to which oxygen-containing species are necessary for the reaction to proceed. Since Ru adsorbs oxygen-containing species at lower potentials than Pt, oxidation of CO_{ads} on bi-metallic Pt–Ru surfaces starts earlier than on pure Pt surface.

Fig. 4(a) shows CO_{ads} stripping voltammogram for Pt/C featuring a symmetrical single oxidation peak at 0.79 V. CO_{ads} oxidation on PtRu/C (Fig. 4(d)) commences earlier, the peak is broad with a maximum at 0.56 V and tails towards positive potentials, as usual for the solid solution of Pt and Ru [38]. However, the CO_{ads} oxidation profiles for $Pt/Ru_{0.1}Ti_{0.9}O_2$ and $Pt/Ru_{0.7}Ti_{0.3}O_2$ are quite different. The catalyst with the lower amount of Ru in the support (Fig. 4(b)) has a pre-peak at 0.4 V followed by the main peak with a maximum at 0.68 V and a shoulder at 0.73 V. CO_{ads} oxidation on $Pt/Ru_{0.7}Ti_{0.3}O_2$ commences at 0.45 V (Fig. 4(c)), similarly as on PtRu/C, but the peak is broader and consist of two overlapping peaks. Earlier onset of CO_{ads} oxidation on $Pt/Ru_{0.1}Ti_{0.9}O_2$ and $Pt/Ru_{0.7}Ti_{0.3}O_2$ comparing with Pt/C and separation of the CO_{ads} oxidation peaks on $Pt/Ru_{0.1}Ti_{0.9}O_2$ and $Pt/Ru_{0.7}Ti_{0.3}O_2$ suggests that some CO molecules are adsorbed onto Pt nanoparticles

in close contact with Ru (oxidation peak at lower potential), while the others are adsorbed onto Pt nanoparticles rather far from Ru (oxidation peak at higher potential) [39]. This observation is in accordance with the results of the EDS elemental maps which suggest that Pt is deposited on both Ru and Ti rich domains on the support.

Integration of the CO_{ads} stripping voltammogram also enables estimation of EASA of Pt and PtRu nanoparticles. By applying the same assumption of 420 μC cm^{-2} for a monolayer, the EASA values obtained from the CO_{ads} stripping match those from the upd Cu within the reproducibility range of ±5%. The average EASA values for synthesized $Pt/Ru_{0.1}Ti_{0.9}O_2$ and $Pt/Ru_{0.7}Ti_{0.3}O_2$ as well for commercial Pt/C and PtRu/C catalysts were calculated according to equation:

$$\mathrm{ECSA} = \frac{Q_{des}}{420\,\mu\mathrm{C\,cm^{-2}} \times w(\mathrm{Pt}) \times m_c} \quad (4)$$

where Q_{des} is the charge under the stripping peaks of upd Cu or CO_{ads}, w(Pt) is the Pt (or PtRu) loading of catalyst (in mass fraction) and m_c is the mass of the catalyst on the electrode. The results of the EASA calculation are summarized in Table 1. As can be seen, the difference between EASA and RSA values for $Pt/Ru_{0.1}Ti_{0.9}O_2$ and $Pt/Ru_{0.7}Ti_{0.3}O_2$ is quite large. This means that Pt utilization, calculated as EASA to RSA ratio, is low. Usual causes of low utilization of Pt are imperfect electrical contact between Pt particles and the support and blockage of a part of the Pt surface attached to the support. Agglomeration of the Pt particles contributes to low Pt utilization as well, because only isolated particles are taken into account for determination of surface-averaged diameter that is used in RSA calculation. Since agglomeration of the Pt particles in the synthesized $Pt/Ru_{0.1}Ti_{0.9}O_2$ and $Pt/Ru_{0.7}Ti_{0.3}O_2$ catalysts (Fig. 2(a) and Fig. S3) is more pronounced than in the commercial Pt/C catalyst [31], the Pt utilization in the synthesized catalysts (21% and 43%) is lower than in the commercial one (68%). Moreover, surface area of the supporting material should also be considered as a factor affecting EASA of Pt. Comparing literature data for the similar catalysts as in our study, a correlation between BET surface area of the support and the EASA of Pt deposited on it can be found. Pt deposited on TiO_2–RuO_2 with BET surface area of 33 m^2 g^{-1} possessed EASA of only 19 m^2 g^{-1} [18], while EASA of Pt deposited on $Ti_{0.7}Ru_{0.3}O_2$ with BET surface area of 276 m^2 g^{-1} was 117 m^2 g^{-1} [19].

3.3. Methanol oxidation on $Pt/Ru_xTi_{1-x}O_2$

The activity of the catalysts for MOR was firstly tested under the potentiodynamic conditions. The electrode was subjected to 250 potential cycles between 0.05 V and 1 V in an electrolyte containing methanol. Although the anode potential in DMFC is usually much lower than the positive limit in this test, in the case of cell reversal caused by fuel starvation [40] the anode catalyst could be exposed to high potential values. Thus, potential cycling conditions simulate such circumstances.

Fig. 5 displays the fifth anodic scan after the addition of methanol in the electrolyte, which is chosen as representative of the initial activity under the potentiodynamic conditions. As can be seen, the onset potential of the reaction at $Pt/Ru_{0.7}Ti_{0.3}O_2$ and PtRu/C is about 0.1 V lower than that of $Pt/Ru_{0.1}Ti_{0.9}O_2$ and Pt/C. Comparing the first two catalysts with low onset potential, the activity of $Pt/Ru_{0.7}Ti_{0.3}O_2$ is higher than the activity of PtRu/C in the entire potential region. Maximum current density attained on $Pt/Ru_{0.7}Ti_{0.3}O_2$ is 0.75 mA cm^{-2}, while on commercial PtRu/C is only 0.2 mA cm^{-2}. It should be noted that the normalization of the current recorded on those two catalysts was not the same, since in the case of PtRu/C the total surface area of PtRu nanoparticles was used, while for $Pt/Ru_{0.7}Ti_{0.3}O_2$ it was the surface of Pt nanoparticles. If the currents for PtRu/C were normalized to Pt surface, they would be roughly double than those presented in Fig. 5 (because of nominal atomic ratio of Pt:Ru of 1:1), but the maximum current density would be still about half of the this for $Pt/Ru_{0.7}Ti_{0.3}O_2$. The MOR curves for the catalysts with high onset potential are almost the same. The current densities for $Pt/Ru_{0.1}Ti_{0.9}O_2$ are higher at the potentials above 0.75 V, but it is irrelevant for a potential application in DMFC. If we turn back to the curve for $Pt/Ru_{0.7}Ti_{0.3}O_2$, it can be conceived as superposition of the currents on PtRu/C and Pt/C, because it starts at low potentials and achieve high currents at higher potentials. A shoulder observed for $Pt/Ru_{0.7}Ti_{0.3}O_2$ is at the same potential of 0.77 V as the peak for PtRu/C, while the current peaks for both Pt/C and $Pt/Ru_{0.7}Ti_{0.3}O_2$ are around 0.9 V. Such a combination of good qualities of PtRu/C and Pt/C catalysts is related to the $Pt/Ru_{0.7}Ti_{0.3}O_2$ structure revealed with elemental mapping (Fig. 2(c)), according to which Pt atoms are deposited on both RuO_2 and TiO_2 domains. On the Pt atoms attached to RuO_2 the MOR is facilitated through bifunctional mechanism. The Pt atoms on TiO_2 behave similar to Pt in Pt/C catalyst, meaning that the onset of the reaction is delayed, but the maximum activity is attained at higher potentials so the currents are larger. The influence of the catalyst structure observed in CO_{ads} oxidation (Fig. 4) is analogous to this in MOR.

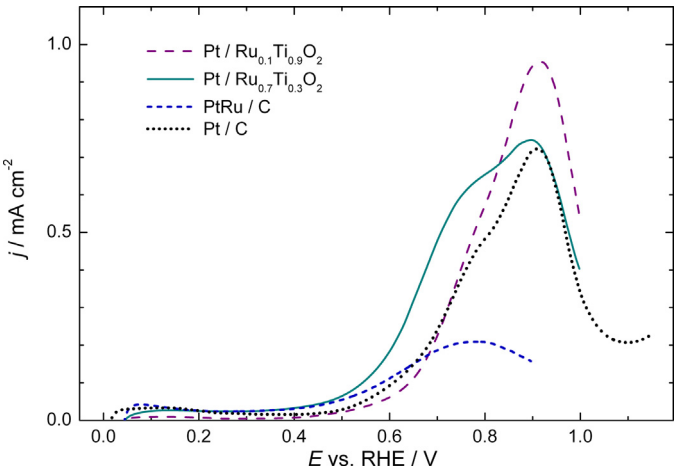

Fig. 5. Potentiodynamic polarization curves for methanol oxidation on $Pt/Ru_{0.1}Ti_{0.9}O_2$, $Pt/Ru_{0.7}Ti_{0.3}O_2$, PtRu/C and Pt/C recorded in the 5th forward scan in 0.1 M H_2SO_4 containing 0.5 M CH_3OH at the scan rate of 50 mV s^{-1}.

The results of the activity test over 250 cycles are presented in Fig. 6. The currents at the potential of 0.5 V taken from the anodic scans were corrected for the background currents estimated at 0.3 V and normalized to EASA determined at the beginning of the experiment. The resulting current densities were plotted as a function of the cycle number. As seen, the activity of $Pt/Ru_{0.1}Ti_{0.9}O_2$ catalyst was low and only slightly better that that of Pt/C over the entire potentiodynamic test. The $Pt/Ru_{0.7}Ti_{0.3}O_2$ catalyst exhibited the highest initial activity, but also rather steep decline in the first 50 cycles. PtRu/C catalyst shows moderate initial activity and slow, almost uniform activity loss, but is the most active from 50th cycle onward. However, at the end of the stability test the activities of $Pt/Ru_{0.7}Ti_{0.3}O_2$ and PtRu/C were almost the same.

The activity of the catalysts during the potentiodynamic test could decrease because of a gradual poisoning of the Pt surface by the methanol oxidation residues and/or because of a loss of the EASA. In order to resolve which effect was predominant, $Pt/Ru_{0.7}Ti_{0.3}O_2$ and PtRu/C catalysts were subjected to potential cycling in the supporting electrolyte containing no methanol. At the beginning and at the end of the experiment, the EASA was determined by CO_{ads} stripping. It was found that both catalysts lost 22% of their initial EASA. Since the decrease in MOR activity was 52%

Table 2
Mass activities for MOR of the $Pt/Ru_{0.1}Ti_{0.9}O_2$, $Pt/Ru_{0.7}Ti_{0.3}O_2$ and PtRu/C catalyst determined under potentiodynamic and potentiostatic conditions.

	Potentiodynamic test at 50 mV s^{-1}				Potentiostatic test at 0.5 V	
	j_{max}/mA mg^{-1}		$j_{0.5\,V}$/mA mg^{-1}		t = 2 min	t = 25 min
	5th cycle	250th cycle	5th cycle	250th cycle		
$Pt/Ru_{0.1}Ti_{0.9}O_2$	251	147	4.6	3.3	1.32	0.99
$Pt/Ru_{0.7}Ti_{0.3}O_2$	345	323	19	8.8	19	12
PtRu/C	292	369	43	28	44	29
Pt/C	526	408	9.1	9.1	5.0	3.9

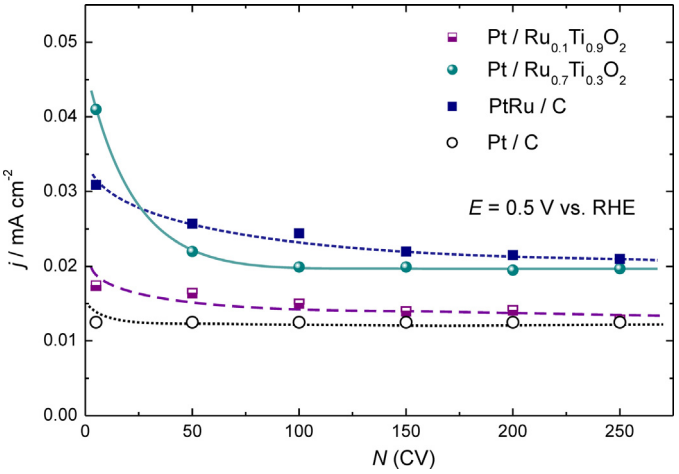

Fig. 6. The current densities for the MOR on $Pt/Ru_{0.1}Ti_{0.9}O_2$, $Pt/Ru_{0.7}Ti_{0.3}O_2$, PtRu/C and Pt/C taken at 0.5 V from the cyclic voltammograms recorded in 0.1 M H_2SO_4 containing 0.5 M CH_3OH at the scan rate of 50 mV s^{-1}.

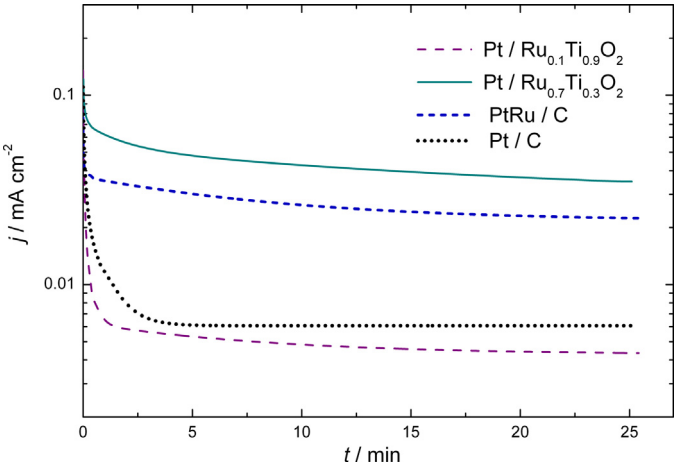

Fig. 7. Chronoamperometric curves of the MOR recorded on $Pt/Ru_{0.1}Ti_{0.9}O_2$, $Pt/Ru_{0.7}Ti_{0.3}O_2$, PtRu/C and Pt/C in 0.1 M H_2SO_4 containing 0.5 M CH_3OH at constant potential of 0.50 V.

for $Pt/Ru_{0.7}Ti_{0.3}O_2$ and 32% for PtRu/C, it seems that poisoning of Pt sites in $Pt/Ru_{0.7}Ti_{0.3}O_2$ is more prominent than in PtRu/C catalyst.

The potentiostatic test was performed during 25 min at the potential of 0.5 V. This potential value was chosen as the upper limit of the anode potential range between 0.3 V and 0.5 V that is considered as relevant for practical DMFC operating conditions [41]. The chronoamperometric curves presented in Fig. 7 show that the lowest current densities are recorded at $Pt/Ru_{0.1}Ti_{0.9}O_2$ and Pt/C, but contrary to the potentiodynamic conditions, $Pt/Ru_{0.7}Ti_{0.3}O_2$ were more active than PtRu/C during the whole test. This result was confirmed in four independent measurements with each catalyst. It is notable that the difference between $Pt/Ru_{0.1}Ti_{0.9}O_2$ and Pt/C, on the one hand, and $Pt/Ru_{0.7}Ti_{0.3}O_2$ and PtRu/C on the other hand, is much larger than observed in the potentiodynamic test. This suggests that $Pt/Ru_{0.1}Ti_{0.9}O_2$ and Pt/C are susceptible to the poisoning by methanol oxidation residues which are oxidatively removed at high potentials during the potential cycling experiment, but remain adsorbed on the Pt nanoparticles if the potential is held close to the onset of the reaction. $Pt/Ru_{0.7}Ti_{0.3}O_2$ and PtRu/C catalysts exhibited better activity probably because majority of their Pt atoms are in close contact with Ru being either in oxide or metallic form, which facilitates removal of the poisoning species from the Pt surface even at a potential as low as 0.5 V.

In order to see whether the adsorbed species remained on the catalysts at the end of the potentiostatic test, the anodic stripping in the supporting electrolyte without methanol was performed. The results (Fig. S5) indicated a presence of adsorbed species on Pt/C and $Pt/Ru_{0.7}Ti_{0.3}O_2$, but not on PtRu/C. According to the oxidation potential, the adsorbed species are probably CO_{ads}. The presence of CO_{ads} on $Pt/Ru_{0.7}Ti_{0.3}O_2$ is to be ascribed to Pt particles attached to TiO_2, because TiO_2 cannot facilitate CO_{ads} oxidation. It is interesting that even at the end of potentiostatic test the activity of $Pt/Ru_{0.7}Ti_{0.3}O_2$ catalyst was high despite a partial coverage of Pt surface by CO_{ads}.

Although current density normalized to the surface area of the electroactive metal (specific activity) is descriptor of the intrinsic activity of a catalyst, the current normalized to the mass of electroactive metal (mass activity) is important for a practical application of a catalyst. The results of potentiodynamic and potentiostatic examination of MOR on $Pt/Ru_{0.1}Ti_{0.9}O_2$, $Pt/Ru_{0.7}Ti_{0.3}O_2$, PtRu/C and Pt/C, expressed as mass activity, are summarized in Table 2.

The performance of $Pt/Ru_{0.1}Ti_{0.9}O_2$ in MOR, either expressed as specific or mass activity, is poor and this catalyst cannot be considered as viable for any practical application. However, comparison of $Pt/Ru_{0.7}Ti_{0.3}O_2$ with the commercial PtRu/C catalyst based on specific activities reveals that their performances are similar, confirming that the bifunctional mechanism is the same regardless of whether Ru is present in the catalyst as metal or oxide [42]. Under the potential cycling conditions $Pt/Ru_{0.7}Ti_{0.3}O_2$ loses its high initial activity, but after about 200 cycles its activity is only slightly lower than that of PtRu/C (Fig. 6). During the potentiostatic test at 0.5 V (Fig. 7) the activity of $Pt/Ru_{0.7}Ti_{0.3}O_2$ exceeds PtRu/C for almost 60% at the end of the test. According to these observations, it can be speculated that high positive potentials are detrimental for the activity of $Pt/Ru_{0.7}Ti_{0.3}O_2$. Dissolution or agglomeration of Pt nanoparticles can be excluded as a cause because potential cycling in the supporting electrolyte showed no significant decline in the EASA. However, since Ru is in different forms in those catalysts (oxide and metallic), it can be assumed that irreversible transformation of Ru-oxides at high positive potentials into a species with lower ability of donating oxygen-containing species contributes to increased activity loss of $Pt/Ru_{0.7}Ti_{0.3}O_2$.

If the mass activities of $Pt/Ru_{0.7}Ti_{0.3}O_2$ and PtRu/C are compared (Table 2), it can be concluded that the maximum currents under the potentiodynamic conditions are similar. However, if data collected at 0.5 V either in potentiodynamic or in potentiostatic conditions are considered, the performance of $Pt/Ru_{0.7}Ti_{0.3}O_2$ is weaker than that of PtRu/C. Having in mind that their specific activities are close to each other (Figs. 6 and 7), lower mass activity of $Pt/Ru_{0.7}Ti_{0.3}O_2$ is a consequence of low Pt utilization caused by Pt particle agglomeration. Therefore, high specific activity of $Pt/Ru_{0.7}Ti_{0.3}O_2$ that characterizes its intrinsic activity towards MOR, indicates that improvement of the Pt particle distribution over the $Ru_{0.7}Ti_{0.3}O_2$ support should render the catalyst suitable for DMFC application.

Although straightforward comparison of data from the studies of different research groups is difficult because of different experimental conditions, we have contrasted our results with the study of MOR on $Pt/Ti_{0.7}Ru_{0.3}O_2$ reported by Ho et al. [19]. It can be calculated that maximum current recorded in cyclic voltammetry on $Pt/Ti_{0.7}Ru_{0.3}O_2$ was 489 mA mg^{-1} or 0,42 mA cm^{-2} if normalized to Pt mass or Pt surface area, respectively. The results for $Pt/Ru_{0.7}Ti_{0.3}O_2$ in the present study show 345 mA mg^{-1} or 0,75 mA cm^{-2}, which confirm that the intrinsic activity of this catalyst is remarkable, but Pt particle distribution needs to be improved in order to achieve good mass activity.

4. Conclusion

Two oxide materials with different Ru content, $Ru_{0.1}Ti_{0.9}O_2$ and $Ru_{0.7}Ti_{0.3}O_2$, were synthesized by an acid-catalyzed sol–gel method. XRD measurements showed that both samples consist of two phases with anatase and rutile structures with anatase predominant in $Ru_{0.1}Ti_{0.9}O_2$ and rutile predominant in $Ru_{0.7}Ti_{0.3}O_2$. Pt nanoparticles were supported on $Ru_{0.1}Ti_{0.9}O_2$ and $Ru_{0.7}Ti_{0.3}O_2$ using borohydride reduction method. According to HAADF-STEM imaging, the surface-averaged diameter of Pt nanoparticles is 3.4 nm for $Pt/Ru_{0.1}Ti_{0.9}O_2$ and 3.7 nm for $Pt/Ru_{0.7}Ti_{0.3}O_2$ catalyst and they are deposited on both Ru and Ti rich domains.

Cyclic voltammetry of $Pt/Ru_{0.1}Ti_{0.9}O_2$ and $Pt/Ru_{0.7}Ti_{0.3}O_2$ catalysts showed characteristics of a clean Pt surface. Oxidation of pre-adsorbed CO was also examined and compared with the samples of commercial Pt/C and PtRu/C catalysts. Based on the onset potential and the structure of the oxidation peaks, it was concluded that in both synthesized catalysts a portion of Pt nanoparticles is in close contact with Ru atoms from the support, which enables the bifunctional mechanism to be operative.

The catalysts were tested for methanol oxidation under the potentiodynamic and potentiostatic conditions. It was revealed that the activity of $Pt/Ru_{0.1}Ti_{0.9}O_2$ is low, but behavior of $Pt/Ru_{0.7}Ti_{0.3}O_2$ was much better. In the potentiodynamic stability test over 250 potential cycles the specific activity of $Pt/Ru_{0.7}Ti_{0.3}O_2$ catalyst was slightly worse than PtRu/C. It was also demonstrated that during the potential cycling in the supporting electrolyte without methanol the decrease of the EASA of $Pt/Ru_{0.7}Ti_{0.3}O_2$ and PtRu/C were both equal to 22%. However, in the potentiostatic stability test at 0.5 V over 25 min the current densities on $Pt/Ru_{0.7}Ti_{0.3}O_2$ exceed those on PtRu/C for about 60%. If the mass activities of $Pt/Ru_{0.7}Ti_{0.3}O_2$ and PtRu/C were compared, the performance of $Pt/Ru_{0.7}Ti_{0.3}O_2$ catalyst was two- or three-fold lower either in potentiodynamic or in potentiostatic test. This is the consequence of lower Pt utilization in $Pt/Ru_{0.7}Ti_{0.3}O_2$ catalyst caused by certain agglomeration of Pt particles on the oxide support.

The present study showed that binary $Ru_xTi_{1-x}O_2$ oxides possess good conductivity and stability in the electrochemical experiments, so they can serve as an electrocatalyst support. However, only the oxides with high Ru content, such as $Ru_{0.7}Ti_{0.3}O_2$, operate as a co-catalyst, enabling efficient methanol oxidation on the supported Pt nanoparticles.

Acknowledgements

This work was financially supported by the Ministry of Education, Science and Technological Development of the Republic of Serbia, Contract No. ON-172054. Transmission electron microscopy was performed at the National Center for Electron Microscopy, which is supported by the Office of Science, Office of Basic Energy Sciences, of the U.S. Department of Energy under Contract No. DE-AC02-05CH11231.

Appendix A. Supplementary data

Supplementary data associated with this article can be found, in the online version, at http://dx.doi.org/10.1016/j.apcatb.2015.01.038.

References

[1] E. Antolini, Appl. Catal. B-Environ. 88 (2009) 1–24.
[2] J. Wang, G. Yin, Y. Shao, S. Zhang, Z. Wang, Y. Gao, J. Power Sources 171 (2007) 331–339.
[3] C.A. Reiser, L. Bregoli, T.W. Patterson, J.S. Yi, J.D. Yang, M.L. Perry, T.D. Jarvi, Electrochem. Solid-State Lett. 8 (2005) A273–A276.
[4] Z. Zhao, L. Castanheira, L. Dubau, G. Berthomé, A. Crisci, F. Maillard, J. Power Sources 230 (2013) 236–243.
[5] H.-S. Oh, J.-H. Lee, H. Kim, Int. J. Hydrogen Energy 37 (2012) 10844–10849.
[6] J.C. Meier, C. Galeano, I. Katsounaros, J. Witte, H.J. Bongard, A.A. Topalov, C. Baldizzone, S. Mezzavilla, F. Schüth, K.J.J. Mayrhofer, Beilstein J. Nanotech. 5 (2014) 44–67.
[7] E. Antolini, E.R. Gonzales, Solid State Ionics 180 (2009) 746–763.
[8] S. Sharma, B.G. Pollet, J. Power Sources 208 (2012) 96–119.
[9] Z. Liu, J. Zhang, B. Han, J. Du, T. Mu, Y. Wang, Z. Sun, Microporous Mesoporous Mater. 81 (2005) 169–174.
[10] S.-Y. Huang, P. Ganesan, S. Park, B.N. Popov, J. Am. Chem. Soc. 131 (2009) 13898–13899.
[11] S.-Y. Huang, P. Ganesan, B.N. Popov, Appl. Catal. B-Environ. 102 (2011) 71–77.
[12] S.-Y. Huang, P. Ganesan, B.N. Popov, Appl. Catal. B-Environ. 96 (2010) 224–231.
[13] S.Lj. Gojković, B.M. Babić, V.R. Radmilović, N.V. Krstajić, J. Electroanal. Chem. 639 (2010) 161–166.
[14] Q. Du, J. Wu, H. Yang, ACS Catal. 4 (2014) 144–151.
[15] L. Chevallier, A. Bauer, S. Cavaliere, R. Hui, J. Roziere, D.J. Jones, ACS Appl. Mater. Interfaces 4 (2012) 1752–1759.
[16] D. Wang, C.V. Subban, H. Wang, E. Rus, F.J. DiSalvo, H.D. Abruña, J. Am. Chem. Soc. 132 (2010) 10218–10220.
[17] O.E. Haas, T.S. Briskeby, O.E. Kongstein, M. Tsypkin, R. Tunold, B.T. Boressen, J. New Mater. Electrochem. Syst. 11 (2008) 9–14.
[18] C.-P. Lo, G. Wang, A. Kumar, V. Ramani, Appl. Catal. B-Environ. 140–141 (2013) 133–140.
[19] V.T.T. Ho, K.C. Pillai, H.-L. Chou, C.-J. Pan, J. Rick, W.-N. Su, B.-J. Hwang, J.-F. Lee, H.-S. Sheub, W.-T. Chuang, Energy Environ. Sci. 4 (2011) 4194–4200.
[20] V.T.T. Ho, N.G. Nguyen, C.-J. Pan, J.-H. Cheng, J. Rick, W.-N. Su, J.-F. Lee, H.-S. Sheu, B.-J. Hwang, Nano Energy 1 (2012) 687–695.
[21] M. Watanabe, S. Motoo, J. Electroanal. Chem. 60 (1975) 267–273.
[22] C. Vericat, M. Wakisaka, R. Haasch, P.S. Bagus, A. Wieckowski, J. Solid State Electrochem. 8 (2004) 794–803.
[23] B. Hammer, Y. Morikawa, J.K. Norskov, Phys. Rev. Lett. 76 (1996) 2141–2144.
[24] C.J. Pelliccione, E.V. Timofeeva, J.P. Katsoudas, C.U. Segre, J. Phys. Chem. C 117 (2013) 18904–18912.
[25] J.S. Spendelow, P.K. Babu, A. Wieckowski, Curr. Opin. Solid-State Mater. Sci. 9 (2005) 37–48.
[26] S. Boujday, F. Wunsch, P. Portes, J.F. Bocquet, C. Colbeau-Justin, Sol. Energy Mater. Sol. Cells 83 (2004) 421–433.
[27] N.R. Elezović, B.M. Babić, V.R. Radmilović, Lj.M. Vračar, N.V. Krstajić, Appl. Catal. B-Environ. 140–141 (2013) 206–212.
[28] K.W. Park, K.S. Seul, Electrochem. Commun. 9 (2007) 2256–2260.
[29] E.P. Barret, L.G. Joyner, P.P. Halenda, J. Am. Chem. Soc. 73 (1951) 373–380.
[30] T.J. Schmidt, H.A. Gasteiger, R.J. Behm, Electrochem. Commun. 1 (1999) 1–4.
[31] I. Esparbé, E. Brillas, F. Centellas, J.A. Garrido, R.M. Rodríguez, C. Arias, P.-L. Cabot, J. Power Sources 190 (2009) 201–209.
[32] S. Lj. Gojković, T.R. Vidaković, D.R. Đurović, Electrochim. Acta 48 (2003) 3607–3614.
[33] C.L. Green, A. Kucernak, J. Phys. Chem. B 106 (2002) 1036–1047.
[34] D. Chen, Q. Tao, L.W. Liao, S.X. Liu, Y.X. Chen, S. Ye, Electrocatalysis 2 (2011) 207–219.

[35] K.T. Jacob, R. Subramanian, J. Phase Equilib. Diffus. 29 (2008) 136–140.
[36] J. Durst, C. Simon, F. Hasché, H.A. Gasteiger, J. Electrochem. Soc. 162 (2015) F190–F203.
[37] H.A. Gasteiger, N. Markovic, P.N. Ross, E.J. Cairns, J. Phys. Chem. 98 (1994) 617–625.
[38] W. Sugimoto, K. Aoyama, T. Kawaguchi, Y. Murakami, Y. Takasu, J. Electroanal. Chem. 576 (2005) 215–221.
[39] Y.Y. Tong, H.S. Kim, P.K. Babu, P. Waszczuk, A. Wieckowski, E. Oldfield, J. Am. Chem. Soc. 124 (2002) 468–473.
[40] A. Taniguchi, T. Akita, K. Yasuda, Y. Miyazaki, J. Power Sources 130 (2004) 42–49.
[41] C. Bock, B. MacDougall, Y. LePage, J. Electrochem. Soc. 151 (2004) A1269–A1278.
[42] H.M. Villullas, F.I. Mattos-Costa, L.O.S. Bulhões, J. Phys. Chem. B 108 (2004) 12898–12903.